TECHNICAL NOTE

Two-Dimensional Filtering of SPECT Images using the Metz and Wiener Filters

Michael A. King, Ronald B. Schwinger, Paul W. Doherty, and Bill C. Penney

The University of Massachusetts Medical Center, Worcester, Massachusetts

Two-dimensional filtering, both before and after reconstruction, has been applied to the processing of single photon emission computerized tomographic (SPECT) images. The filters investigated were the count-dependent Metz filter and Wiener filter, both of which automatically adapt to the image being processed. Using a SPECT phantom, with images reconstructed with these filters rather than the ramp, we observed a statistically significant increase ($p < 0.05$) in the image contrast for solid Plexiglas spheres, and significant decrease ($p < 0.05$) in the percent fractional standard deviation of counts in a region of uniform activity. The adaptability of these filters is demonstrated by a comparison of SPECT acquisitions of the phantom at two different count levels. An example of their application to clinical studies is presented. We conclude that two-dimensional digital image restoration with these techniques can produce a significant increase in SPECT image quality, with a small cost in processing time when these techniques are implemented on an array processor.

J Nucl Med 25: 1234–1240, 1984

The increased contrast sensitivity and improved three-dimensional visualization provided by single photon emission computerized tomography (SPECT) holds the promise of improving early detection and delineation of disease states with radionuclide imaging (*1*). However, the image quality provided by SPECT has limited SPECT's fulfillment of its anticipated role. SPECT image quality has been less than optimal because of a number of factors including technical problems with instrumentation, the problem of attenuation correction, and a high noise level with inadequate spatial resolution (*1–6*). An approach to the problems of noise and spatial resolution through the use of digital image processing after acquisition is the subject of this paper.

The use of digital filters is an integral part of the reconstruction of SPECT images by filtered backprojection (*2–9*). In the frequency domain, the filter used usually involves a ramp function, which corrects for the blurring inherent in backprojection, multiplied by a function that determines the portion of the ramp to be used. This second function is usually termed the "window" function. A number of window functions have been proposed (*2–9*). Typically, one-dimensional window functions have been used, probably because much of the work on tomographic reconstruction was done in transmission tomography, where data are collected from only one slice at a time. In nuclear medicine, two-dimensional images are acquired, and consequently the use of two-dimensional windows has been proposed (*10,11*). Until recently the amount of time required to perform two-dimensional filtering of the data has been excessive. The use of array processors markedly decreases the processing time for such techniques (*12*), resulting in clinically acceptable execution times on a dedicated nuclear medicine computer system.

Window functions have usually been low-pass digital filters that roll off smoothly toward zero at high spatial frequencies in order to avoid ripple artifacts (*7*) and to suppress high-frequency terms dominated by noise. The use of resolution recovery filters that enhance selected frequencies to compensate for their attenuation during acquisition has been suggested (*6*). The image power spectrum—which is the square of the complex magnitude of the two-dimensional Fourier transform of the image—can be modeled as consisting of the sum of the power spectrum of the blurred object plus that of the noise (*13–15*). It has been demonstrated that as the number of counts in an image increases, the object power spectrum can be differentiated from the noise power spectrum to a greater extent in the frequency domain (*13–15*). Thus the frequency at which the window function begins to roll off should move to higher spatial frequencies, with increased counts. Also, the form of the window should be influenced by the object power spectrum, since it is the combination of object power spectrum and the noise

Received Jan. 18, 1984; revision accepted June 20, 1984.

For reprints contact: Michael A. King, PhD, Dept. of Nuclear Medicine, The University of Massachusetts Med. Ctr., Worcester, MA 01605.

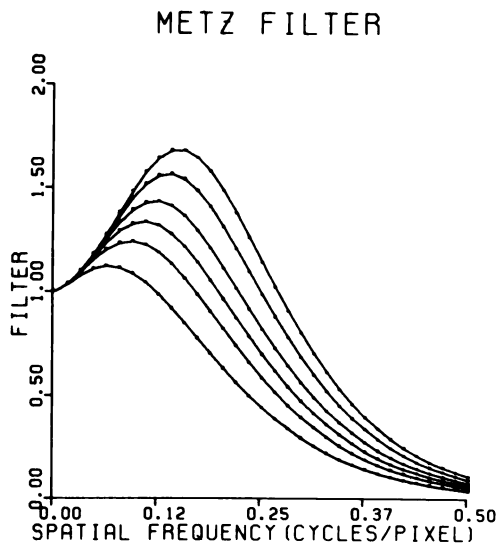

FIG. 1. Plot of Metz filter used for processing SPECT images, for total counts of 20,000, 50,000, 100,000, 200,000, 500,000, and 1 million from lowest to highest curve.

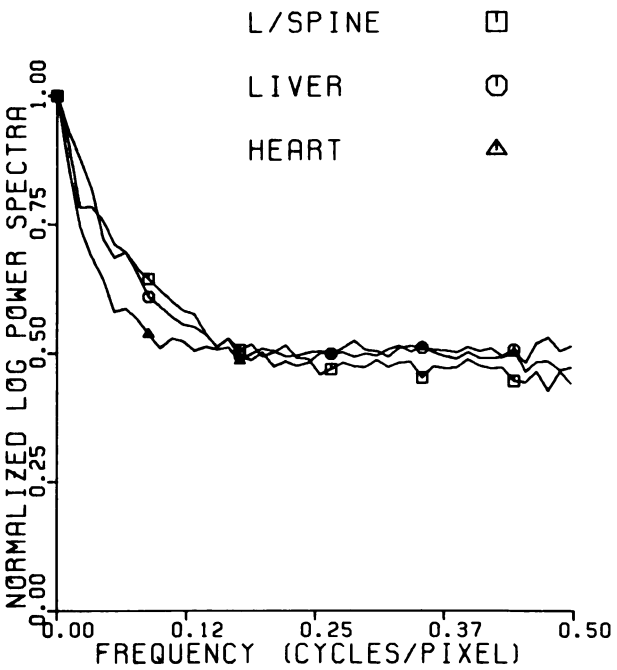

FIG. 2. Comparison of logarithm of power spectra of three different types of SPECT images (bone study of lumbar spine, liver/spleen study, and gated heart blood-pool SPECT study).

level that determines to what extent the object can be differentiated from the noise (*13–15*). Therefore, there is no unique window function for use with SPECT; instead, one of a family of "optimal" functions should be selected automatically by an algorithm based on some parameter(s) of the image to produce "optimal" image quality. Promising preliminary results along this line have been reported with one-dimensional implementations of the Wiener filter in the spatial (*16*) or frequency (*17*) domain.

The purpose of this work was to evaluate the effect of using two-dimensional filtering of SPECT images on image quality. We studied two filter types that automatically adapt to the image being processed. A comparison was also made of the effect of using these filters both before and after reconstruction, and at different count levels.

METHODS

Two restoration filters that adapt to the images being processed were investigated, for use as two-dimensional window functions for preprocessing SPECT images and in filtering reconstructed images. In both cases, each filter was first formed as a one-dimensional function of spatial frequency, which was then used to generate two dimensionally symmetric filters. This was accomplished by forming the two-dimensional filter as a function of radial displacement from the origin (zero frequency). All of the filtering was carried out in the frequency domain by multiplying the two-dimensional Fourier transform of the image by the filter, and then inverse-transforming the result.

Metz filter. The first filter investigated was the count-dependent Metz filter (*14,18,19*), whose one-dimensional form is defined as:

$$M(f) = MTF(f)^{-1} \cdot [1 - (1 - MTF(f)^2)^X], \quad (1)$$

where MTF is the modulation transfer function, f is the spatial frequency, and X is a factor that controls the extent to which the inverse filter is followed before the filter switches to noise suppression (*14*). That is, the filter is made up of the product of the inverse filter [first term after equal sign in Eq. (1)] and a low-pass filter (second term), and the magnitude of X determines the frequency at which the low-pass filter begins to dominate. X was made a function of the total image count, being optimized to give the minimum mean square error (MSE) for a set of simulated two-dimensional object/image pairs (*14*). This causes the filter to adapt to the image being reconstructed. It was observed that lower MSE values, and visually more pleasing images, could be obtained by using a generalized exponential function instead of the "true" MTF in Eq. (1) (*14*). The form of this exponential function and details on its "optimization", have been published (*14*). This filter was used to process SPECT studies either before or after reconstruction by filtered backprojection. The only change made from previous applications of this filter (*14*) was to alter the filter to compensate for the increased pixel size due to the use of a larger crystal (38 cm compared with 27 cm diameter) and variations in magnification when using the camera.

Figure 1 shows the one-dimensional form of this filter, plotted for six different total image counts. Notice that, as the count increases, more resolution recovery occurs (filter rises farther above 1.0), together with less noise suppression (filter moves farther to the right). In Fig. 2 the logarithm of the power spectrum of several SPECT acquisition images, of ~50,000 total counts each, is plotted against spatial frequency. Two-dimensional power spectra have been averaged over annuli to yield the one-dimensional functions plotted in this figure. The filter second from the bottom in Fig. 1 would be used for filtering the studies of Fig. 2. Note that this filter falls below 1.0 at about the same spatial frequency that the object power spectra of Fig. 2 blend with that of the noise power spectra. This is the frequency at which the image power spectra become "flat", indicating that the noise components are now dominating those of the object (*15*).

Wiener filter for planar images. The second filter investigated was the Wiener. For images degraded by Poisson noise, the one-dimensional form of this filter has been shown to be (*13,15,20,21*):

$$W(f) = MTF^{-1}(f) \cdot MTF^2(f)/[MTF^2(f) + \bar{N}/P_0(f)], \quad (2)$$

where $\bar{N}$ is the total image count, which for Poisson noise is equal to the average value of the noise power spectrum, and P_0 is the object power spectrum. As with the Metz filter, the Wiener is made

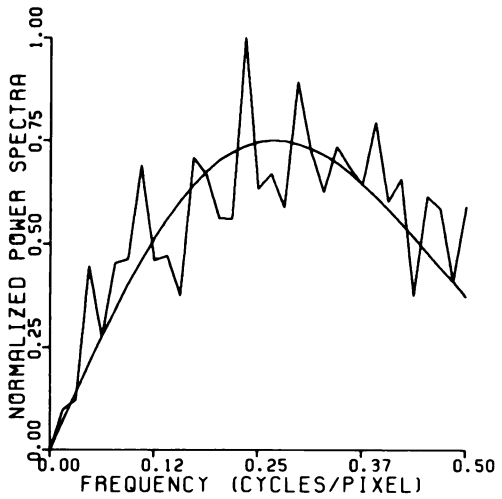

FIG. 3. Plot of logarithm of noise power spectrum in reconstruction of simulated uniform-count phantom, and predicted form for ramp filter and linear interpolation.

up of the product of the inverse filter and a low-pass filter. The roll-off of the low-pass filter is dependent on the magnitude of the ratio of the noise to object power spectra, compared with the square of the MTF. Thus this filter adapts to images of different objects as well as to different noise levels.

In order to form the Wiener filter it is necessary to have estimates of the object power spectrum, noise power spectrum, and MTF. The method for obtaining these estimates and implementing the Wiener filter for planar images has been described (*15*). The MTF used in generating the Wiener filter for SPECT studies was obtained as the Fourier transform of a Gaussian function fitted to the reconstruction of a line source at the center of rotation, acquired with acquisition parameters (collimator, magnification, and radius of rotation) matching those of the study to be filtered.

Wiener filter for reconstructed SPECT slices. The noise power spectrum of the acquisition data is altered by the processes of filtering, backprojection, and interpolation during reconstruction (*6,22,23*). For Shepp-Logan "window" functions and linear interpolation (*3*), the theoretical form of the noise power spectrum (P_n), as a one-dimensional function of spatial frequency, is (*22,23*):

$$P_n(f) = (MN/\pi) f \, \mathrm{SINC}^2(\pi f/f_c) \, \mathrm{SINC}^4(\pi f a), \qquad (3)$$

where f_c is the cutoff frequency of the filter, a is the pixel size, and SINC is defined as SIN X over X; it is assumed that M projections each backproject a total count N. Equation (3) does not account for attenuation or its correction. To test Eq. (3), we reconstructed a simulated acquisition of a uniform phantom, with the projections degraded by Poisson noise. No account of attenuation was taken in obtaining the simulated acquisition data, nor were attenuation-compensation techniques used in reconstructing the image. The results are shown in Fig. 3 for a ramp filter and linear interpolation. Notice the good agreement between predicted and actual values for the noise power spectrum. The form of the noise power spectrum of Eq. 3 was subtracted from the image power spectrum to yield an estimate of the object power spectrum for use in forming the Wiener filter used in postprocessing SPECT images (*24*). In the actual implementation, a least-squares fit of Eq. (3) to the end of the image power spectrum was used. This assumes that the object power spectrum reduces to insignificance at high frequencies. We have observed this to be approximately true for clinical images (Fig. 2), but, as one might expect, not for high-count images of SPECT phantoms, which are highly structured and contain fine detail.

Comparison of image quality. To assess the effects of these filters upon image quality, the following study was performed. Five SPECT acquisitions of a standard SPECT phantom* (64 frames of 64 × 64 pixels each) at each of two different count levels (200,000 and 20,000 per frame) were acquired using a single-head, rotating camera SPECT system interfaced to a nuclear medicine computer system. The count levels were chosen to span the levels encountered clinically. An asymmetric energy window was used to reduce scatter (*25*). A high-resolution collimator and a circular head orbit of 14 cm radius were used for image acquisition. The full width at half maximum of the system with this collimator and radius of rotation was 1.4 cm. To reduce the possible effects of aliasing with a 64 × 64 acquisition matrix (*26,27*), a magnification factor of 1.5 was used, resulting in a pixel size of 0.4 cm. The images were reconstructed using standard software† adapted to run

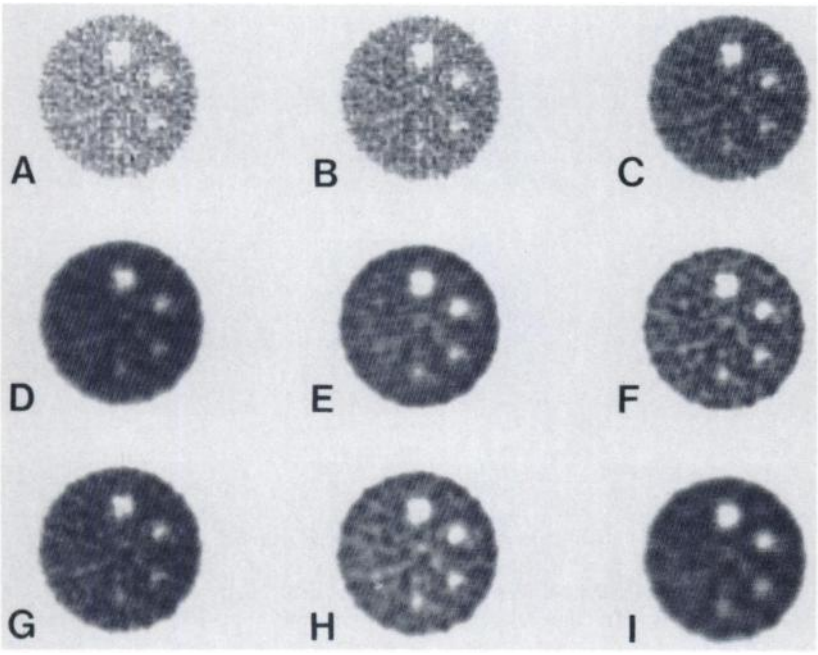

FIG. 4. Slices from acquisition of SPECT phantom, at 200,000 counts per frame, with six Plexiglas spheres with diameters of 0.95, 1.27, 1.59, 1.91, 2.54, and 3.18 cm, spaced 60° apart. A: ramp; B: Shepp-Logan-2; C: Shepp-Logan-4; D: Shepp-Logan-5; E: Metz prefilter; F: Wiener prefilter; G: ramp followed by 9-point smooth of slice; H: Metz postfilter; and I: Wiener postfilter.

TABLE 1. IMAGE CONTRAST AND FRACTIONAL STANDARD DEVIATION FOR 200,000 COUNTS PER ACQUISITION FRAME

Filter	Image contrast				% Fract. SD	
	1.59* cm	1.91* cm	2.54* cm	3.18* cm	Center†	Periphery†
Ramp	0.36	0.45	0.62	0.72	17.6	14.4
	(0.15)	(0.10)	(0.08)	(0.08)	(2.1)	(1.6)
Shepp-Logan-1‡	0.36	0.45	0.62	0.72	16.8	13.6
	(0.14)	(0.09)	(0.08)	(0.08)	(1.9)	(1.5)
Shepp-Logan-2‡	0.34	0.44	0.61	0.72	14.5§	11.5§
	(0.13)	(0.08)	(0.07)	(0.08)	(1.5)	(1.3)
Shepp-Logan-3‡	0.31	0.43	0.60	0.71	11.4§	8.8§
	(0.10)	(0.07)	(0.06)	(0.08)	(0.8)	(1.1)
Shepp-Logan-4‡	0.28	0.41	0.59	0.71	8.6§	6.8
	(0.08)	(0.05)	(0.05)	(0.07)	(0.2)	(1.2)
Shepp-Logan-5‡	0.23	0.36	0.54	0.68	4.9§	3.6§
	(0.04)	(0.03)	(0.03)	(0.05)	(0.6)	(0.7)
Metz prefilter	0.36	0.56	0.83§	1.00§	7.4§	5.1§
	(0.06)	(0.04)	(0.04)	(0.01)	(0.5)§	(1.3)
Metz postfilter	0.45	0.66§	0.90§	0.98§	10.2§	7.4§
	(0.10)	(0.05)	(0.06)	(0.02)	(0.7)	(1.5)
Wiener prefilter	0.40	0.60§	0.85§	0.97§	10.0§	6.7§
	(0.10)	(0.07)	(0.07)	(0.04)	(0.5)	(0.9)
Wiener postfilter	0.30	0.43	0.66	0.86§	7.1§	4.9§
	(0.05)	(0.02)	(0.03)	(0.07)	(1.2)	(0.9)

* Average (s.d.) image contrast for five different acquisitions at this count level.

† Average (s.d.) % FSD for counts in 5- by 5-pixel region of interest over center or periphery of slices from five different acquisitions at this count level.

‡ Shepp-Logan filters of increasing softness.

§ Significantly different ($p < 0.05$) from ramp filter.

on an array processor.‡ Attenuation correction was done using the arithmetic-mean method (*3*). The images were reconstructed using a ramp filter, five different Shepp-Logan filters (*3*), and two-dimensional Metz and Wiener filtering followed by reconstruction with the ramp filter, or with the ramp filter and then processed using either the Metz or Wiener filters. For a three-pixel-wide slice through a set of solid spherical Plexiglas lesions, the magnitude of the image contrast was defined as (*5,28*):

$$C_{image} = \frac{[\text{counts/pixel}_{(lesion)} - \text{counts/pixel}_{(background)}]}{\text{counts/pixel}_{(background)}}, \quad (4)$$

and was calculated for spheres of 1.59, 1.91, 2.54, and 3.18 cm in diameter. To assess the effects of filtering on noise levels, we calculated the percent fractional standard deviation (% FSD) for 5- by 5-pixel regions of interest (ROIs) in the center and at the periphery of a three-pixel-wide slice through a phantom containing uniform activity. For a given sphere or ROI used for calculating % FSD, the statistical significance of the variation in the mean image contrasts or % FSD between the filters was determined using a one-way analysis of variance (*29,30*). When a significant difference was observed between the means of the various filters at a p value of 0.05 or less, Sheffe's method of comparing paired means for a significant difference (*29,30*) was used to compare the results of each of the other nine filters with the ramp filter.

RESULTS

With our system it requires ~0.2 sec to filter two-dimensionally a 64- by 64-pixel image with the Metz filter including disk I/O, and 18 sec to filter a 64-frame SPECT acquisition. This is to be compared with 130 sec to process a single 64- by 64-pixel image without the array processor or floating-point hardware (*12*). Similarly, it requires about 3 sec to form the filter and to filter two-dimensionally a 64- by 64-pixel image with the Wiener filter, and 4 min to process an entire 64-frame SPECT acquisition. The difference in processing time between the two techniques can be almost eliminated if the Wiener filter is formed for only the first of 64 frames of a SPECT acquisition, and the same filter is then applied to the rest of the frames.

The results of the quantitative comparison of the filters in terms of their effect upon image contrast and % FSD are given in Tables 1 and 2, and a comparison can be obtained visually in Fig. 4. The tables show that the two-dimensional processing techniques produce both a significant increase in image contrast and reduction in the % FSD, compared with the ramp filter. The decrease in noise can be seen in two ways. First by a decrease in % FSD, and second by a decrease in the standard deviations of the image contrast. The latter is important because it means not only that the average image contrast is improved with the two-dimensional restoration techniques, but also that the variation in the contrast is also diminished. Thus the spheres are seen with greater certainty.

The count-dependent nature of the Wiener and Metz filtering techniques can be seen in that, at the higher count level, the filters adapt to produce a smaller reduction in % FSD and a greater improvement in image contrast. This is to be compared with the Shepp-Logan filters, which produced approximately the same fractional decrease in % FSD at both count levels. The behavior of the count-dependent Metz filter can be studied in more detail

TABLE 2. IMAGE CONTRAST AND FRACTIONAL STANDARD DEVIATION FOR 20,000 COUNTS PER ACQUISITION FRAME

Filter	Image contrast				% Fract. s.d.	
	1.59* cm	1.91* cm	2.54* cm	3.18* cm	Center†	Periphery†
Ramp	0.17	0.24	0.59	0.74	45.0	46.2
	(0.23)	(0.24)	(0.15)	(0.16)	(4.1)	(3.1)
Shepp-Logan-1‡	0.16	0.25	0.60	0.75	43.1	44.3
	(0.22)	(0.24)	(0.15)	(0.16)	(3.8)	(2.8)
Shepp-Logan-2‡	0.14	0.27	0.61	0.78	37.8§	38.8§
	(0.19)	(0.25)	(0.15)	(0.14)	(3.2)	(2.0)
Shepp-Logan-3‡	0.11	0.30	0.63	0.82	30.0§	30.4§
	(0.16)	(0.24)	(0.15)	(0.13)	(2.4)	(1.3)
Shepp-Logan-4‡	0.10	0.33	0.63	0.85	21.9§	21.8§
	(0.12)	(0.20)	(0.15)	(0.12)	(2.1)	(2.3)
Shepp-Logan-5‡	0.08	0.30	0.59	0.81	12.5§	12.1§
	(0.09)	(0.09)	(0.09)	(0.15)	(1.6)	(2.74)
Metz prefilter	0.18	0.44	0.77	0.97§	15.7§	13.9§
	(0.11)	(0.15)	(0.13)	(0.06)	(3.0)	(4.9)
Metz postfilter	0.14	0.39	0.74	0.89	17.0§	16.2§
	(0.13)	(0.11)	(0.08)	(0.10)	(1.9)	(4.2)
Wiener prefilter	0.12	0.33	0.60	0.86	10.8§	9.7§
	(0.08)	(0.10)	(0.10)	(0.11)	(1.9)	(3.4)
Wiener postfilter	0.14	0.23	0.48	0.67	5.7§	5.7§
	(0.06)	(0.07)	(0.08)	(0.13)	(1.0)	(1.3)

* Average (s.d.) image contrast for five different acquisitions at this count level.

† Average (s.d.) % FSD for counts in a 5- by 5-pixel region of interest over center or periphery of slices from five different acquisitions at this count level.

‡ Shepp-Logan filters of increasing softness.

§ Significantly different ($p < 0.05$) from ramp filter.

with the help of Fig. 1. In the high-count acquisition images there are 200,000 counts per frame, thus the prereconstruction Metz filter used would be fourth from the bottom of Fig. 1. There were approximately 1.2 million counts per slice in the reconstructions of this phantom, thus the postreconstruction Metz filter used would be the top one of Fig. 1. The change in filters with count level explains, in part, the higher contrasts and noise levels in the images filtered after reconstruction (Table 1). A similar analysis for the low-count acquisition data of Table 2 shows again a lower noise level for prereconstruction filtering, but it also shows a higher contrast. This may be a reflection of a slight advantage for prereconstruction filtering due to the addition of information in adjoining slices.

In comparing the two-dimensional restoration filters, we find that our method of Wiener postreconstruction processing produces the least contrast enhancement and the most noise suppression. This results, in part, from the adaptability of the Wiener filter to changes in object power spectrum, since the object power spectrum of the slices was observed to have less high frequency content than that of the acquisition frames. There are only relatively small differences between the remaining three methods of two-dimensional processing. In these a small increase in contrast is generally coupled with a similar increase in noise (% FSD) making the choice between them difficult.

We have found these techniques useful clinically. Figure 5 illustrates the effect on image quality for a liver/spleen SPECT study in which there were approximately 50,000 counts per acquisition frame. As seen in this figure and quantified in Table 3, prereconstruction processing using the Metz and Wiener filters reduces the % FSD in the liver, and increases lesion contrast.

DISCUSSION

Digital filtering of SPECT images is currently performed by selecting, from a list of one-dimensional filters, a window function to use in reconstruction, viewing the resulting image slices, and then repeating the process by selecting a different window function if the results are unsatisfactory. The two-dimensional image restoration techniques investigated in this study automatically adapt to the image being processed, and thus eliminate the need for repeated reconstructions. They have been shown to produce a significant increase in image contrast and a reduction in noise level, compared with reconstructions using the ramp filter, all at the cost of only a slight increase in execution time (approximately 18 sec) when an array processor is used.

Figure 4 shows that besides an alteration in the noise magnitude as determined by the % FSD, the noise character or structure (*19,31*) is also altered with application of the different filters. This results because not only are the frequency components of the object being altered by the filters, but—as was shown in the discussion with Eq. (3)—the noise components are also being filtered. Thus noise "blobs" can appear, which might interfere with the process of detection of small lesions. This fact should be kept in mind whenever digital filtering is used, and filters should be chosen to minimize the potential for this hazard.

The choice between prereconstruction and postreconstruction

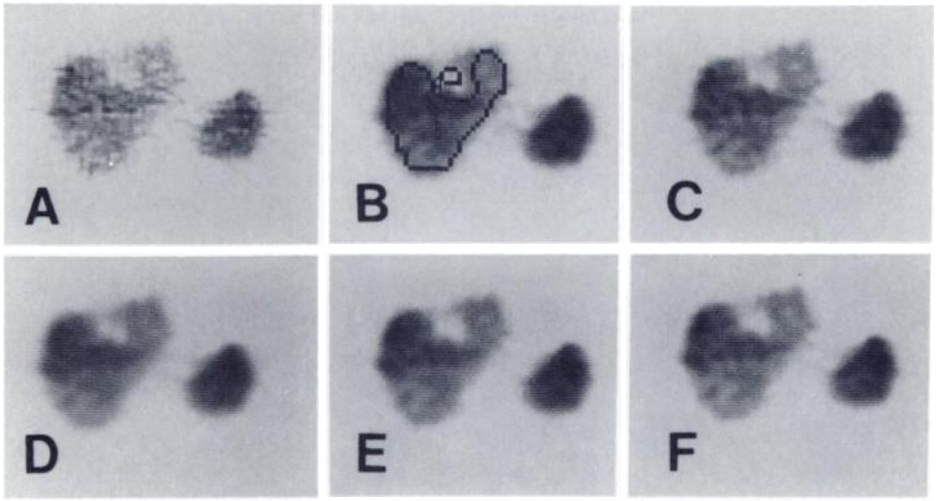

FIG. 5. Slices from SPECT liver/spleen study reconstructed using: (A) ramp, (B) ramp plus 9-point smooth with ROIs superimposed, (C) Shepp-Logan-4, (D) Shepp-Logan-5, (E) Metz prefilter, and (F) Wiener prefilter.

filtering of SPECT studies is not entirely clearcut, as is illustrated in Tables 1 and 2. We tend to favor prereconstruction filtering for the following reasons. First, the noise power spectrum of the planar image is easier to estimate than that of SPECT images (*6,22,23*). Second, with two-dimensional prereconstruction filtering, a larger statistical sample is used to determine the value supplied to the backprojector at each point (i.e., the whole data set is filtered, not just one slice). This is important, since SPECT imaging is photon-limited (*2–6*), and the additional information contained in nearby slices can help to reduce noise and increase contrast, as is illustrated by the low-count data of Table 2. Third, the blurring of nuclear medicine images is two-dimensional, hence it is clear that techniques for two-dimensional resolution recovery should be utilized to preprocess acquisition data. This and the larger statistical sample allow better input data to be supplied to the backprojector, thereby resulting in better SPECT images. Finally, for the reconstruction of oblique-angle slices from transverse slices, prereconstruction filtering with a two-dimensionally symmetric filter produces an image with an isotropic point response (*11*). We have verified that for a given spatial location the full width at half maximum varies only about one mm in any direction for images reconstructed by these filters.

There are also some advantages, however, for postreconstruction filtering. One advantage of postreconstruction processing for recovery of resolution is that spatial resolution (MTF) varies much less across a given tomographic slice than it does with distance away from the face of a collimator in planar images. This makes the use of a single MTF with deconvolution more appropriate. Also, only the slices actually reconstructed need to be processed. With an array processor to minimize execution time this is of minimal importance, but when a minicomputer alone is used, the time saving could be significant.

The choice between Wiener and count-dependent Metz filtering is difficult. The Wiener filter has a sound theoretical basis and adapts to noise level, object power spectrum, and image blur (system MTF) for the image being processed (*15–17,20*). The count-dependent Metz filter, as implemented, adapts only to changes in noise level (*14*), but because of its simplicity it does have a speed advantage over the Wiener filter. With clinical images we have found no great difference in image quality between the use of either of these techniques to filter SPECT images (Fig. 5). This may be a reflection of the relatively small difference in object power spectra for many clinical nuclear medicine images (Fig. 2), compared with the variation caused by different total counts, and it may also be because both filters used the minimization of the MSE as their criterion for optimality.

TABLE 3. LESION CONTRAST AND FRACTIONAL STANDARD DEVIATION IN RECONSTRUCTED SLICE OF LIVER

Filter	% Lesion contrast	Liver % FSD
Ramp	60.5	27.1
Ramp plus 9-point smooth	55.9	18.6
Shepp-Logan-4	57.6	19.4
Shepp-Logan-5	54.7	17.9
Metz prefilter	66.6	18.0
Wiener prefilter	66.5	18.2

CONCLUSION

In this paper we have presented a comparison of two methods of image-dependent two-dimensional filtering of SPECT images. It is apparent that significant improvements in image quality can be obtained with two-dimensional filtering techniques that adapt to the image. It is our belief that even more improvement can be obtained with use of the more powerful techniques of digital image processing.

FOOTNOTES

* Data Spectrum Deluxe "SPECT Phantom."
† DEC SPETS-11 Reconstruction Software Package.
‡ Analogic AP400 Array Processor.

ACKNOWLEDGMENTS

The authors thank Mr. Steven Cool and Dr. Tom Miller for their advice and encouragement. We also thank Linda Desai for her assistance in the preparation of this paper. This investigation was aided by Biomedical Research Support Grant S07RR5712.

REFERENCES

1. KEYES JW: Perspectives on tomography. *J Nucl Med* 23: 633-640, 1982
2. BUDINGER TF, GULLBERG GT, HUESMAN RH: Emission computed tomography. In *Image Reconstruction From Projections* Herman OT, ed. New York, Springer-Verlag, 1979, pp 147-246
3. LARSSON SA: Gamma camera emission tomography. *Acta Radiol* (Suppl) 363:1-15, 1980
4. BUDINGER TF: Physical attributes of single-photon tomography. *J Nucl Med* 21:579-592, 1980
5. JASZCZAK RJ, COLEMAN RE, WHITEHEAD FR: Physical factors affecting quantitative measurements using camera-based single photon emission computed tomography (SPECT). *IEEE Trans Nucl Sci* 28:69-80, 1981
6. TODD-POKROPEK A: The mathematics and physics of emission computerized tomography (ECT). In *Emission Computed Tomography: Current Trends.* Esser P, ed. New York, Society of Nuclear Medicine, 1983, pp 3-31
7. CHESLER DA, RIEDERER SJ: Ripple suppression during reconstruction in transverse tomography. *Phys Med Biol* 20:632-636, 1975
8. KWOH YS, REED IS, TRUONG TK: A generalized |W|-filter for 3-D reconstruction. *IEEE Trans Nucl Sci* 24: 1990-1995, 1977
9. HUANG S, PHELPS ME, HOFFMAN EJ, et al: Cubic splines for filter design in computed tomography. *IEEE Trans Nucl Sci* 27:1368-1374, 1980
10. WILLIAMS DL, RITCHIE JL, HARP GP, et al: Preliminary characterization of the properties of transaxial whole-body single-photon tomography: Emphasis on future application to cardiac imaging. In *Functional Mapping of Organ Systems And Other Computer Topics.* Esser P, ed. New York, Society of Nuclear Medicine, 1981, pp 149-166
11. GULLBERG GT: True three-dimensional reconstruction in single photon emission computed tomography. *J Nucl Med* 24:P81, 1983 (abstr)
12. KING MA, DOHERTY PW, ROSENBERG RJ, et al: Array processors: An introduction to their architecture, software, and applications in nuclear medicine. *J Nucl Med* 24: 1072-1079, 1983
13. KIRCH DL, BROWN DW: Nonlinear frequency domain techniques for enhancement of radionuclide images. In *Information Processing in Scintigraphy.* USERDA Conf-730687, 1973, pp 102-114
14. KING MA, DOHERTY PW, SCHWINGER RB, et al: Fast count-dependent digital filtering of nuclear medicine images: Concise communication. *J Nucl Med* 24:1039-1045, 1983
15. KING MA, DOHERTY PW, SCHWINGER RB,: A Wiener filter for nuclear medicine images. *Med Phys* 10:876-880, 1983
16. CHO Z, BURGER J: Construction, restoration, and enhancement of 2 and 3-dimensional images. *IEEE Trans Nucl Sci* 24:886-893, 1977
17. TSUI ET, BUDINGER TF: A stochastic filter for transverse section reconstruction. *IEEE Trans Nucl Sci* 26:2687-2690, 1979
18. METZ CE: A mathematical investigation of radioisotope scan image processing. Ph.D. Thesis, University of Pennsylvania, 1969
19. METZ CE, BECK RN: Quantitative effects of stationary linear image processing on noise and resolution of structure in radionuclide images. *J Nucl Med* 15:164-170, 1974
20. GOODMAN JW, BELSHER JF: Fundamental limitations in linear invarient restoration of atmospherically degraded images. In *SPIE* Vol. 75 *Imaging Through The Atmosphere*, Society of Photo-Optical Instrumentation Engineers, 1976, pp 141-154
21. LO CM, SAWCHUK AA: Nonlinear restoration of filtered images with Poisson noise. In *Applications of Digital Image Processing III*, vol. 207, Society of Photo-Optical Instrumentation Engineers, 1976, pp 84-95
22. RIEDERER SJ, PELC NJ, CHESLER DA: The noise power spectrum in computed x-ray tomography. *Phys Med Biol* 23:446-454, 1978
23. HANSON KM, BOYD DP: The characteristics of computed tomographic reconstruction noise and their effect on detectability. *IEEE Trans Nucl Sci* 25:160-163, 1978
24. KING MA, SCHWINGER RB, DOHERTY PW: Fast Wiener digital post-processing of SPECT images. *J Nucl Med* 24: P81-82, 1983 (abstr)
25. KING MA, SCHWINGER R, ESSER P, et al: Preliminary characterization of the properties of a new rotating SPECT imaging system. In *Emission Computed Tomography: Current Trends.* Esser P, ed. New York, Society of Nuclear Medicine, 1983, pp 91-104
26. CASTLEMAN KR: *Digital Image Processing.* Englewood Cliffs, Prentice Hall, 1979, pp 230-238
27. ROSENFELD A, KAK AC: *Digital Picture Processing*, Second Edition, vol. 1, New York, Academic Press, 1982, pp 83-92, 383-389
28. JASZCZAK RJ, WHITEHEAD FR, LIM CB, et al: Lesion detection with single-photon emission computed tomography (SPECT) compared with conventional imaging. *J Nucl Med* 23:97-102, 1982
29. SNEDECOR GW, COCHRAN WG: *Statistical Methods.* Sixth Edition, The Iowa State University Press, Ames, 1967, pp 258-271
30. BROWNLEE KA: *Statistical Theory and Methodology.* Second Edition, New York, John Wiley and Sons, 1965, pp 309-318
31. PIZER SM, TODD POKROPEK AE: Noise character in processed scintigrams. In *Information Processing in Scintigraphy*, Commissariat a l'Energie Atomique, Orsay, 1975, pp 198-213